Tungsten inert gas bead-on-plate weld chemical composition analysis by laser-induced breakdown spectroscopy

IOP Conf. Series: Materials Science and Engineering **882** (2020) 012023 doi:10.1088/1757-899X/882/1/012023

Tungsten inert gas bead-on-plate weld chemical composition analysis by laser-induced breakdown spectroscopy

U A Taparli[1], T Kannengiesser[1,2] and A Griesche[1]

[1] Federal Institute for Materials Research and Testing (BAM), Unter den Eichen 87, 12205 Berlin, Germany
[2] Otto-von-Guericke University Magdeburg, Faculty of Mechanical Engineering, Institute of Materials and Joining Technology, Universitätsplatz 2, 39106 Magdeburg, Germany

ugur-alp.taparli@bam.de

Abstract. Chemical compositions of a weld can be varying locally as a result of the welding process. These local variations can be due to the vaporization of individual alloying elements. In this work, tungsten inert gas (TIG) bead-on-plate stainless steel welds of EN grade 1.4404 and 1.4435 were investigated using laser-induced breakdown spectroscopy (LIBS) on the completed welds. This study aims to reveal the welding parameters' influence on the resulting local chemical compositions of the stainless steel welds. We demonstrated Mn vaporize before Cr due to its lower latent enthalpy of vaporization. Hence, Mn accumulates on the heat-affected zone (HAZ) both sides across the weld bead by being swept away through the circulation flow of the welding plasma. Additionally, increasing the heat input tends to enhance the accumulated Mn content on the HAZ as well as increasing the shielding gas flow rate. The results are in good agreement with the literature and proved that LIBS is an effective method to inspect completed welds.

1 Introduction

Tungsten inert gas (TIG) welding process uses a free burning electric arc in a surrounding shielding gas between a non-consumable tungsten electrode and a workpiece. Consequently, the strong heat flux from the welding arc plasma partially melts the workpiece and forms a weld pool. Metal vapor can be released from the weld pool surface due to the vaporization of the molten material[1]. If the material's loss results in a critical change of the chemical composition, the mechanical properties of the weld may be impaired. Moreover, the chemical composition of the metal vapor and the arc plasma alters the arc stability and fume formation[2].

The alloying elements' vaporization from the weld pool is a complex process and includes several stages. Moreover, the rate of vaporization depends on the relative contributions of each following step. First, the alloying elements are transported to the surface of the weld pool either by convection or diffusion. Second, as the alloying element reaches the surface, several thermodynamic factors determine the rate of vaporization e.g. the local concentration of the alloying element, the extend of surface coverage by the surface active elements, the nature of the weld pool surface interface and the weld pool surface turbulence. Finally, the nature of the boundary layer and the diffusivities of the vaporized species influence the rate of vaporization[3]. The principal factors governing the rate of vaporization including various interdependent physical phenomena are e.g. the temperature distribution at the surface of the

weld pool, partial pressure of the gas species above the weld pool, the chemical composition of the melt, individual elements' molecular weight and their diffusion coefficients[4].

Various experimental and numerical simulation studies have been conducted on the topic of alloying element vaporization to determine the metal vapor behaviour during welding. Yamamoto *et al*. have used a numerical model for TIG welding of stainless steel and concluded the concentration of the manganese in the arc plasma is much higher than the amount of manganese in the stainless steel, especially above the area with the lower weld pool temperature (farther locations from the welding arc) due to the higher partial pressure of manganese at lower temperatures[5]. Tanaka et al. have detected most of the chromium and manganese vapor released from the stainless steel weld pool surface are carried into a circulation flow in the welding plasma (cathode jet) and then swept away towards the surroundings of the welding arc. They have also concluded that if the concentration gradient in the arc plasma is large enough, chromium could be transported through the cathode jet by diffusion and could be carried towards the welding electrode[6]. Tashiro et al. have investigated the fume formation mechanism and the individual particle behaviour in stationary TIG-welding of pure iron. Hence, they observed the metal vapor escaping from the plasma arc to the atmosphere, instantaneously cooling down and condensing as fume[7]. Tanaka et al. have used imaging spectroscopy to observe stationary TIG welding processes and metal vaporization. They have detected that the atomic and ionic chromium are the dominant species in the welding arc plasma compared to iron due to the lower ionisation energy of Cr[8]. Taparli et al. have detected post-weld manganese enrichment at the heat affected zone (HAZ) in stainless steels using laser-induced breakdown spectroscopy (LIBS)[9]. In situ monitoring of the stationary weld pool using LIBS has also indirectly revealed the significant amount of manganese in the metal vapor above the weld pool and instantaneous condensation on the weld metal as soon as the welding process was terminated[10].

Laser-induced breakdown spectroscopy is one of the various methods in atomic emission spectroscopy. It is based on measuring the element specific photon emission. A pulsed laser beam is focused onto the surface of the substance to be analysed. Radiation energy is locally coupled into the material. Consequently, the material starts to evaporate. In this material vapor and the surrounding atmosphere, a plasma is generated, leading to the excitation of the material constituents and their spontaneous emission (Bremsstrahlung). As the plasma cools down and decays with time, it starts to emit element-specific radiation. This emission can be resolved and detected by a spectrometer[11].

This work presents post weld chemical composition analysis results of TIG bead-on-plate stainless steel welds using LIBS. Individual welds were investigated (after the welding process is completed) by perpendicular (to the welding direction) LIBS line-scans to determine the final chemical compositions in the fusion zone (FZ), heat affected zone and the base material. Furthermore, the influence of the welding heat (energy) input and the shielding gas (Ar) flow rate on the final chemical compositions of the welds were investigated.

2 Materials and methods

2.1 Materials

EN grade 1.4404 and 1.4435 (standardized in DIN EN 10088-1) austenitic stainless steels were chosen as sample materials for the experimental series. Chemical compositions of the main alloying elements are shown in Table 1. The values were measured by conventional mobile spark optical emission spectroscopy instrument Spektrotest (SPECTRO Analytical Instruments GmbH).

Table 1. Selected sample materials and their alloying element concentrations. (Source: Spark-OES)

Grade / Batch (EN 10088-1)	Thickness (*t*) (mm)	Chemical composition (wt%)						
		C	Si	Mn	Cr	Ni	Mo	Fe
1.4404 / 31785	3	0.013	0.33	0.75	17.02	11.11	2.18	bal.
1.4404 / 327005	6	0.021	0.33	1.39	16.84	10.00	2.00	bal.
1.4435 / 315821	4	0.023	0.49	1.49	17.92	12.55	2.47	bal.

Sample plates with the dimensions 320 mm x 35 mm x *t* manufactured by Columbus Stainless Ltd.(1.4435), Outokumpu (1.4404 / 31785) and U&A (1.4404 / 327005) were used for the experiments. The respective surface of the plates was in as-manufactured condition without further mechanical treatment. Prior to welding, they had been cleaned with acetone to remove any resultant surface contaminants.

2.2 Experimental set-up

The LIBS system consisted of a 1064 nm Nd:YAG laser at 10 Hz pulse repetition rate with output energy of 200 mJ (Quantel CFR 200). The laser source was synchronized by a LIBS controller (Lasertechnik Berlin (LTB), Berlin Germany) with the Echelle spectrometer Aryelle 200 (LTB) equipped with intensified charged-coupled device (ICCD) detector (ANDOR iStar, Oxford Instruments). ICCD-detectors have a better time resolution to detect the very short lifetime of the laser-induced plasma (typically lies between 0.5-50µs[11]) and a higher gate-width flexibility compared to single CCD-type detectors[12].

Welding experiments were conducted using a tungsten inert gas (TIG) arc welding system by Castolin CastoTIG 1611DC power supply and Castolin TIG torch using WC-20 tungsten electrode (2% Ceriated) with 1.6 mm diameter. The contact distance from the base material to the electrode tip was set to approx. 3 mm. The electrode tip extended 3 mm from the ceramic gas nozzle (diameter 6 mm). Welding processes were conducted using a motorized linear stage. Sample plates were mounted on the stage and moved, whereby the welding torch and the LIBS system remained fixed. Relative movement of the sample plate resulted in weld beads of 80 mm in length. Welding parameters (welding current and speed) were arranged in order to realise various heat input values. Argon 5.0 (purity ≥ 99.999 %) was used as the shielding gas.

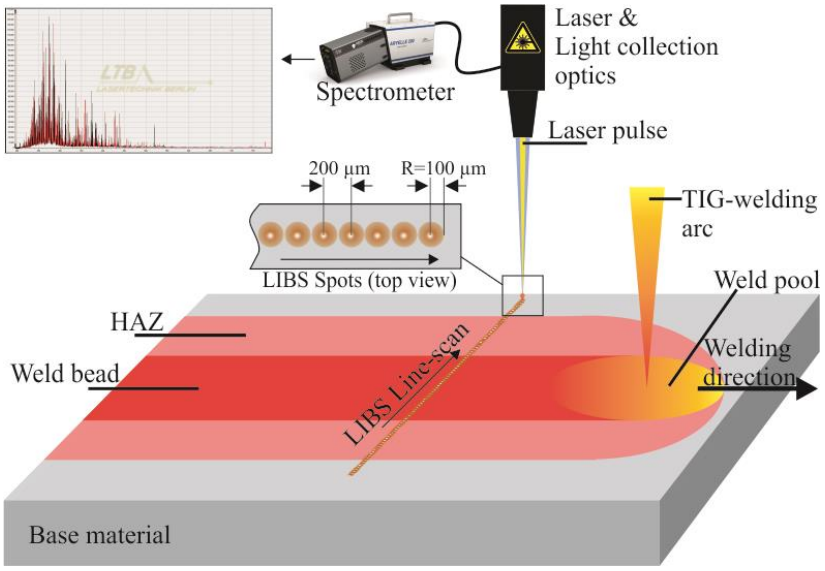

Figure 1. Experimental set-up.

The laser head was positioned normal to the sample surface. The laser beam was focused on the sample surface using a custom-built focusing and light collecting optics system (Figure 1). The emitted light was transmitted into the spectrometer through an optical fibre. A single measurement accumulated the emitted light from 10 laser shots. The delay time between the laser pulse and the beginning of exposure was set to 1.0 μs and ICCD gate width (how long the ICCD gate is open for each LIBS measurement) was set to 20 μs. LIBS line-scans were conducted perpendicular to the welding direction and at the midpoint (at approx. 40 mm from the start) of each weld seam, using the motorized linear stage with a step size of 200 μm. Individual LIBS measurement spots have radii of approx. r = 100 μm.

3 Results and discussion

Each LIBS measurement provides an individual spectrum for that specific measurement spot. Data processing was conducted for each spectrum in the following sequence; the spectral background was removed and individual peaks were fitted using the Gaussian function. Integrating the selected peaks results in the relative intensity values of the selected element. Using a selection of certified reference materials (CRM) and measuring their relative intensity values, one can establish a quantification model for the measured unknown substances and predict their chemical compositions. In this study, we used the basic linear regression method using CRMs to establish the quantified chemical composition values. Further reading on the topic can be found elsewhere[13, 14].

3.1 Space-resolved elemental distributions of Cr and Mn

Processing each spectrum of the line scan results in a chemical composition vs. position profile for each weld seam. Figure 2 demonstrates three processed spectra between approx. 402.8 nm to 403.8 nm (the welding parameters for the sample are indicated in the caption of Figure 2.). These spectra show the typical Mn I triplet peaks at 403 nm, which were also used for quantification of the manganese element in this study. These peaks were processed as it was explained in the previous section i.e. the spectral background was removed; the data were fitted by the Gaussian function and the area under the peak was calculated by definite integral of the curve. In Figure 2, one can see three spectra, however two of them overlap; namely the black curve (measured spectrum from the weld bead) and the blue curve (measured spectrum from the base material) are hard to distinguish. The reason for this can be seen in Figure 3, i.e. the Mn content at the base material and the weld bead are largely similar. However, Mn content for the HAZ is significantly greater compared to the weld bead and the base material. This result indicates that a higher Mn content was observed at the border of the FZ. Moreover, Mn accumulates on the HAZ as a result of the welding process. The spectrum in Figure 2 (red curve), respectively the Mn I peaks recorded from the HAZ, supports this argument with much higher relative intensity values compared to the other two curves.

Figure 3 reveals a slightly different trend for Cr. The chemical compositions present the lowest values for the weld bead or the FZ, and slightly higher values towards the base material (farther away from the FZ). This phenomenon indicates a possible Cr depletion in the solidified weld metal. This can be explained by a possible vaporization of the alloying element in this region. However, contrary to Mn, a significant local accumulation of Cr at any specific location does not occur.

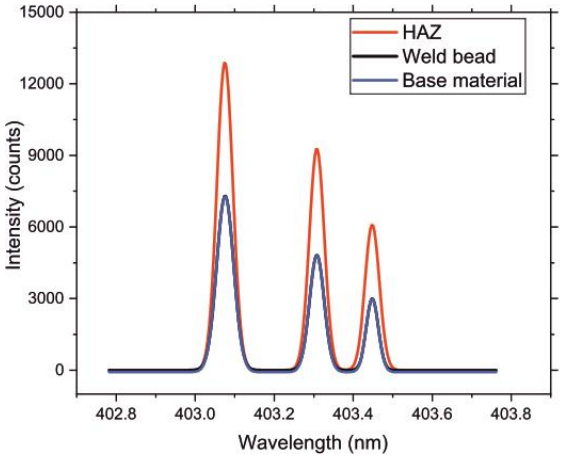

Figure 2. Fitted Mn I triplet peaks around 403 nm. Curves for the "weld bead" and "base material" overlap due to the similar chemical composition values. (EN 1.4404 / 327005 – Welding parameters: welding current = 65A, welding speed = 10 cm/min (Heat input= 491 J/mm), shielding gas flow rate = 18 l/min).

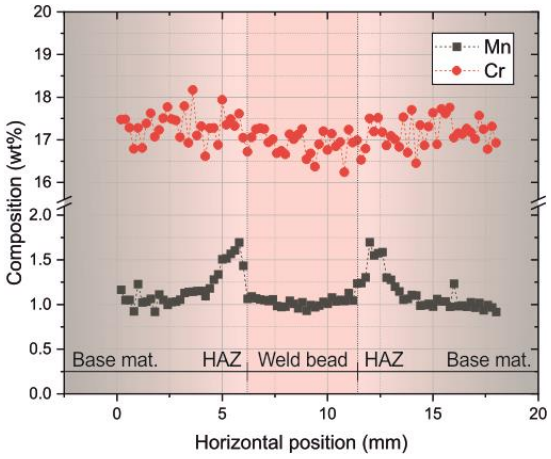

Figure 3. Space-resolved distribution of Cr and Mn elements on the LIBS line-scan perpendicular to the welding direction.

These results for both Mn and Cr are in good agreement with the literature[7-9]. Therefore, we extended our study to investigate the influence of the welding parameters on the local chemical composition changes.

3.2 Relation between welding heat input and Mn accumulation at the HAZ

The previous section has revealed a possible Mn accumulation phenomenon at the HAZ. Hence, the Cr compositions at the FZ differs slightly from the rest of the welds. Figure 4 presents the Mn (left) and Cr (right) compositions as a function of welding heat input for the material EN 1.4404 / 31785. Both diagrams demonstrate the chemical composition of the aforementioned elements measured in three pre-defined locations on the welds (base material, HAZ and weld bead (FZ)).

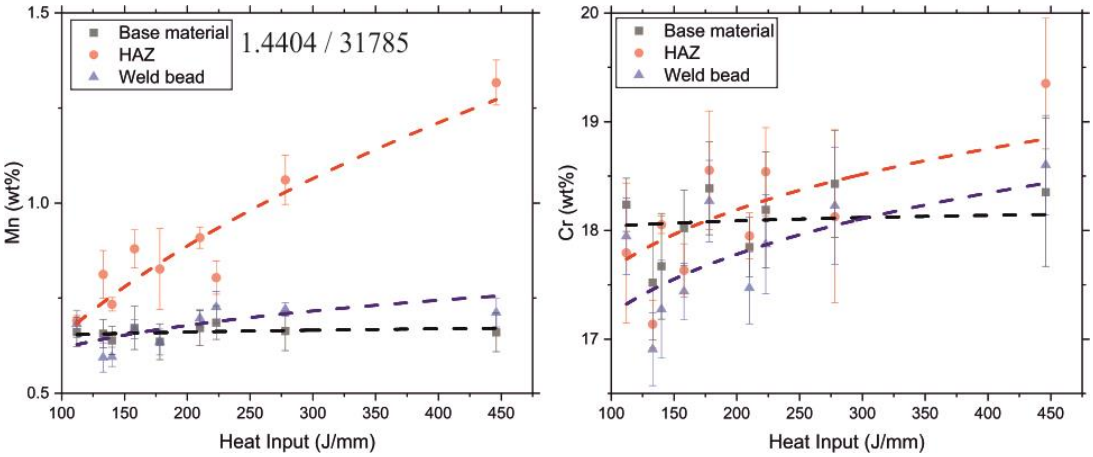

Figure 4. Mn (left) and Cr (right) chemical compositions at the base material, HAZ and the weld bead displayed as a function of welding heat input. Dashed lines are guide-to-the-eye.

Figure 4 shows that increasing the heat input from 110 J/mm up to 450 J/mm results in approx. 0.5 wt% increase of the resulting chemical compositions for both Mn and Cr at the HAZ. Similarly, at the weld bead (FZ) an increasing trend for Mn and Cr compositions with the increasing heat input is observed. However, this latter increasing trend for Mn at the weld bead is relatively slower than for Cr (blue dashed lines). Measurements conducted at the base material have showed only negligible composition variations as function of the heat input (black dashed lines).

Khan et al. reported that increasing the power input during laser welding of stainless steels increases the vaporization rate of individual elements [4]. Their results are in good agreement with the Figure 4. Hence, the Mn composition at the HAZ increases with the higher welding heat input values. Consequently, the amount of the condensed material on the weld surface after welding is also increased. Same principal applies for Cr but in a different location on the weld surface. Tanaka et al. have demonstrated that Cr is dominantly present in the welding arc plasma due to its lower ionisation energy. [8]. It has also been reported that the vaporized Cr could be carried towards the TIG welding electrode[6], which supports the finding of higher Cr composition directly above the weld bead or on the FZ.

3.3 Shielding gas flow rate and alloying element vaporization

This last section presents the chemical composition changes of Mn and Cr as a function of the shielding gas (Ar) flow rate for the sample material 1.4435 / 315821 at constant heat input (491 J/mm). Figure 5 (left) demonstrates the accumulated higher Mn content at the HAZ for any given flow rate with approx. 0.2 wt% increase. The significant increase occurs at the highest applied gas flow rate (20 l/min) with approx. 1 wt% difference to values measured at the base material and the weld bead (FZ). This result also indicated that the vaporized Mn is swept away from the area above the FZ faster and carried onto the HAZ, i.e. also accumulated on the HAZ faster therefore resulting in higher composition value.

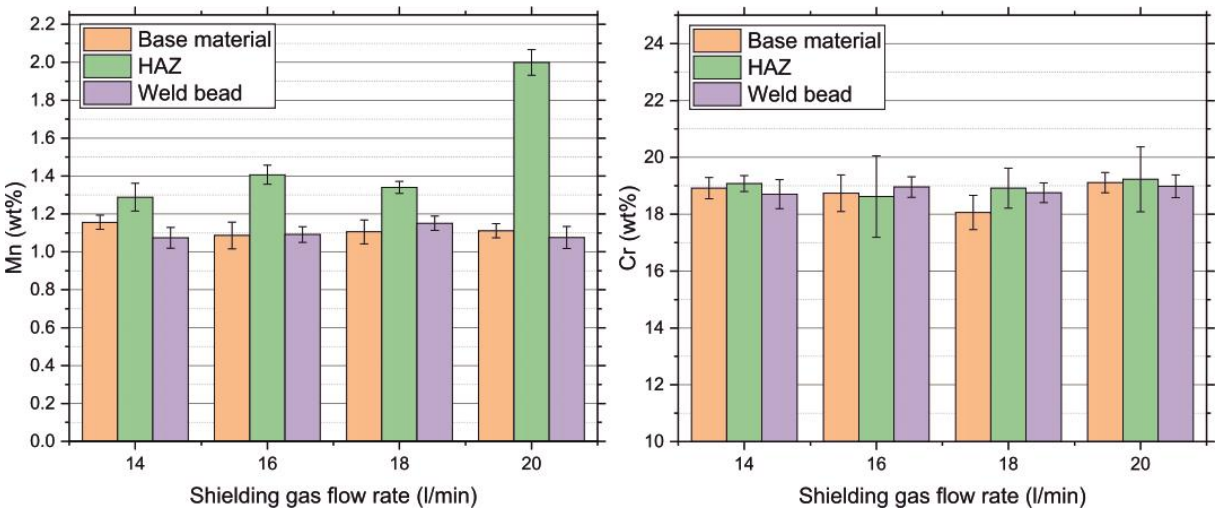

Figure 5. Various shielding gas flow rates and alloying element compositions on the bead-on-weld samples for Mn (left) and Cr (right). (EN 1.4435 / 315821 – Heat input = 491 J/mm constant).

Furthermore, previous in situ LIBS investigations had demonstrated the vaporization rate of the Mn is related to the welding input energy, hence the overall thickness of the accumulated Mn layer was enhanced at higher heat input values[10]. However, this result indicates that the transport model of the individual alloying elements in the welding arc plasma is also strongly related to the shielding gas flow rate, although the rates of vaporization is considered as independent of the gas flow rate in the arc plasma[3]. Considering the rate of vaporization is independent of the gas flow rate, it is possible to interpret this higher Mn content at 20 l/min setting to the faster transport kinetics in the welding arc plasma; not due to the higher vaporization rate.

Cr has demonstrated relatively stable results throughout the all selected flow rate settings for this sample material. The measured chemical composition of the Cr in various areas depend neither on the shielding gas flow rate nor the heat input. Moreover, comparing the latent enthalpy of vaporization values for Mn and Cr would make this assumption more comprehendible. Mn would require 225 kJ/mol to vaporize whereby Cr would need 347 J/mol[15]. Hence, this supports the possible Mn vaporization and consequent condensation to happen thermodynamically easier compared to Cr. Furthermore, Huber et al. reports that the temperature of the weld pool has a high impact on the metal vapor generation and the excitation degree of the individual alloying elements[16]. In this example, the welding heat input possibly lies below the critical level, therefore a distinguishable Cr composition difference on the weld metal was not observed.

4 Conclusions

Laser-induced breakdown spectroscopy method was used to investigate post TIG bead-on-plate welds and the possible metal vaporization and condensation phenomena due to the welding process. Key findings of the study are:

- Mn vaporize from the weld pool during welding and tend to be swept away from the welding arc along the weld bead. Instantaneously, it condenses on the HAZ and resulting in higher chemical compositions across both sides of the weld bead.
- Increasing the heat input results in higher Cr composition on the weld bead (FZ).
- Increasing the heat input results in higher Mn composition on the HAZ.
- Increasing shielding gas flow rate enhanced the Mn content accumulated at the HAZ.

We investigated post-weld individual trends of alloying elements chemical compositions for the selected stainless steel sample materials. The detected phenomena are in good agreement with the literature and the theory. Further research on online LIBS feedback for welding process regulation is in development.

Acknowledgements

Authors would like to thank Lasertechnik Berlin GmbH (LTB) for the analytical equipment. U.A. Taparli would like to thank Mr. Lars Jacobsen (LTB) for his contribution to the data processing.

References

[1] Park H, Trautmann M, Tanaka K, Tanaka M, Murphy A B. A computational model of gas tungsten arc welding of stainless steel: the importance of considering the different metal vapours simultaneously. 2018 *J. Appl. Phys.* **51**(39):395202.

[2] Blockbolten A, Eagar T W. Metal Vaporization from Weld Pools. 1984 *Metall Trans B*.15(**3**):461-9.

[3] Collur M M, Paul A, Debroy T. Mechanism of Alloying Element Vaporization during Laser-Welding. 1987 *Metall Trans B*.;**18**(4):733-40.

[4] Khan P A A, Debroy T. Alloying Element Vaporization and Weld Pool Temperature during Laser-Welding of AISI 202 Stainless-Steel. 1984 *Metall Trans B*.**15**(4):641-4.

[5] Yamamoto K, Tanaka M, Tashiro S, Nakata K, Yamazaki K, Yamamoto E, et al. Numerical Simulation for TIG Welding of Stainless Steel with Metal Vapor. 2008 *The International Conference on Computational & Experimental Engineering and Sciences*. **7**(1):1--6.

[6] Tanaka M, Tsujimura Y, Yamazaki K. Dynamic Behaviour of Metal Vapour in ARC Plasma During TIG Welding. 2012 *Weld World*.**56**(1):30-6.

[7] Tashiro S, Zeniya T, Yamamoto K, Tanaka M, Nakata K, Murphy AB, et al. Numerical analysis of fume formation mechanism in TIG welding. 2015 *Weld Int.* **29**(3):165-72.

[8] Tanaka K, Shigeta M, Tanaka M, Murphy AB. Investigation of the bilayer region of metal vapor in a helium tungsten inert gas arc plasma on stainless steel by imaging spectroscopy. 2019 *J. Appl. Phys.* **52**(35):354003.

[9] Taparli U A, Jacobsen L, Griesche A, Michalik K, Mory D, Kannengiesser T. In situ laser-induced breakdown spectroscopy measurements of chemical compositions in stainless steels during tungsten inert gas welding. 2018 *Spectrochim Acta B.* **139**:50-6.
[10] Taparli U A, Kannengiesser T, Cieslik K, Mory D, Griesche A. In situ chemical composition analysis of a tungsten-inert-gas austenitic stainless steel weld measured by laser-induced breakdown spectroscopy. 2020 *Spectrochim Acta B*. **167**:105826.
[11] Noll R. 2012 *Laser-induced breakdown spectroscopy fundamentals and applications*. (Berlin: Springer).
[12] Mueller M, Gornushkin I B, Florek S, Mory D, Panne U. Approach to Detection in Laser-Induced Breakdown Spectroscopy. 2007 *Anal Chem.* **79**(12):4419-26.
[13] Hahn D W, Omenetto N. Laser-Induced Breakdown Spectroscopy (LIBS), Part I: Review of Basic Diagnostics and Plasma—Particle Interactions: Still-Challenging Issues within the Analytical Plasma Community. 2010 *Appl Spectrosc.* **64**(12):335A-6A.
[14] Hahn D W, Omenetto N. Laser-Induced Breakdown Spectroscopy (LIBS), Part II: Review of Instrumental and Methodological Approaches to Material Analysis and Applications to Different Fields. 2012 *Appl Spectrosc.* **66**(4):347-419.
[15] Zhang Y M, Evans J R G, Yang S F. Corrected Values for Boiling Points and Enthalpies of Vaporization of Elements in Handbooks. 2011 *J Chem Eng Data.* **56**(2):328-37.
[16] Huber S, Glasschroeder J, Zaeh M F. Analysis of the Metal Vapour during Laser Beam Welding. Lasers in Manufacturing 2011 *Proceedings of the Sixth International WLT Conference on Lasers in Manufacturing* **12**, 712-9.